applied sciences

MDPI

Article

Bioresorption Control and Biological Response of Magnesium Alloy AZ31 Coated with Poly-β-Hydroxybutyrate

Lu Wang [1,2], Raffaella Aversa [3], Zhengjun Houa [1], Jie Tian [1], Shuang Liang [1], Shuping Ge [1,4], Yu Chen [2], Valeria Perrotta [3], Antonio Apicella [3,*], Davide Apicella [3], Luigi Cioffi [5] and Guixue Wang [1,*]

1 Key Laboratory for Biorheological Science and Technology of Ministry of Education, State Key Laboratory of Mechanical Transmission, State and Local Joint Engineering Laboratory for Vascular Implants, Bioengineering College of Chongqing University, Chongqing 400044, China; wang_lu_66@126.com (L.W.); houzj@cqupt.edu.cn (Z.H.); tianjie19900228@126.cn (J.T.); bluetears1580@163.com (S.L.); liangs@cqu.edu.cn (S.G.)
2 School of Biological Information, Chongqing University of Posts and Telecommunications, Chongqing 400065, China; gjc@cqupt.edu.cn
3 Advanced Materials Lab., Department of Architecture, Industrial Design University of Campania, Via San Lorenzo, 81031 Aversa, Italy; raffaella.aversa@unicampania.it (R.A.); valeria.perrotta@unicampania.it (V.P.); dott.davide.apicella@outlook.it (D.A.)
4 School of Chemistry and Chemical Engineering, Chongqing University of Technology, Chongqing 400044, China
5 Orthopaedical and Traumatological Center (CTO), Department of Ortho-Neurological and Zonal Trauma Center, 80131 Naples, Italy; luigi.cioffi@ospedalideicolli.it or luigilucacioffi@tin.it
* Correspondence: antonio.apicella@unicampania.it (A.A.); wanggx@cqu.edu.cn (G.W.)

Citation: Wang, L.; Aversa, R.; Houa, Z.; Tian, J.; Liang, S.; Ge, S.; Chen, Y.; Perrotta, V.; Apicella, A.; Apicella, D.; et al. Bioresorption Control and Biological Response of Magnesium Alloy AZ31 Coated with Poly-β-Hydroxybutyrate. *Appl. Sci.* **2021**, *11*, 5627. https://doi.org/10.3390/app11125627

Academic Editor: Giuliana Muzio

Received: 9 May 2021
Accepted: 11 June 2021
Published: 18 June 2021

Featured Application: Tunable bioactive and bioresorbable metal implants.

Abstract: Magnesium and its alloys are not normally used as bioresorbable temporary implants due to their high and uncontrolled degradation rate in a physiological liquid environment. The improvement of corrosion resistance to simulated body fluids (SBF) of a magnesium alloy (AZ31) coated with poly-β-hydroxybutyrate (PHB) was investigated. Scanning electron microscopy, Fourier transform infrared spectrometer, and contact angle measurements were used to characterize surface morphology, material composition, and wettability, respectively. pH modification of the SBF corroding medium, mass of Mg^{2+} ions released, weight loss of the samples exposed to the SBF solution, and electrochemical experiments were used to describe the corrosion process and its kinetics. The material's biocompatibility was described by evaluating the effect of corrosion by products collected in the SBF equilibrating solution on hemolysis ratio, cytotoxicity, nitric oxide (NO), and total antioxidant capacity (T-AOC). The results showed that the PHB coating can diffusively control the degradation rate of magnesium alloy, improving its biocompatibility: the hemolysis rate of materials was lower than 5%, while in vitro human umbilical vein endothelial cell (HUVEC) compatibility experiments showed that PHB-coated Mg alloy promoted cell proliferation and had no effect on the NO content and that the T-AOC was enhanced compared with the normal group and bare AZ31 alloy. PHB-coated AZ31 magnesium alloy extraction fluids have a less toxic behavior due to the lower concentration of corrosion byproducts deriving from the diffusion control exerted by the PHB coating films both from the metal surface to the solution and vice versa. These findings provide more reference value for the selection of such systems as tunable bioresorbable prosthetic materials.

Keywords: bioresorbable implants; magnesium alloy; PHB; biocompatibility; cytotoxicity; NO; temporary implants

1. Introduction

Biological implants have been widely used in various applications, and most of these biomedical devices are made from different biomaterials designed to stay permanently

in the body. However, due to complications such as long-term endothelial dysfunction, delayed reendothelialization, late thrombosis, permanent physical irritation, toxic metal ion release, and local chronic inflammation, such long-term implantations often need secondary surgeries to remove them [1–4].

Several bioresorbable materials have been therefore proposed to overcome these long-term limitations associated with permanent implant materials, and among these, magnesium is still attracting significant attention for its light weight, good mechanical properties, and compatibility with human physiology [5].

Another intriguing characteristic of magnesium is its osteoconductive activity, which has been described to occur in clinical trials as an increase of bone apposition in magnesium-based implants [6]. Since early studies [7,8], it has been assessed that the presence of Mg structures for human bone fracture reduction decreases the time for hard callous formation. The presence of Mg ions is a crucial cofactor for many enzymatic metabolic activities [6,7] that facilitate tissue healing [8]. Moreover, even when in excess, Mg ions do not often cause cellular toxicity since they are readily expelled with body excretions.

Unfortunately, pure magnesium is not directly suitable for such applications due to its insufficient mechanical and corrosion properties. Magnesium alloys have been considered to overcome most of these difficulties [8–16]. However, not all of them could be considered as proper materials for resorbable medical implants, especially those containing high concentrations of elements such as zirconium, aluminum, and rare earth metals that may induce inflammatory cascades and tissue damage [5,15–20]. The magnesium alloy AZ31, which is characterized by a relatively low content of aluminum (3%) and zinc (1%), has been experimentally proved to possess good biocompatibility [11,12].

Due to its good balance among mechanical, biocompatibility, and biodegradation characteristics, Mg AZ31 alloy may be a suitable bioresorbable implant material. However, it should be considered that because several clinical treatments, such as bone healing, may require up to 12 weeks to complete [5], material with more reliable and controlled corrosion kinetics should be adopted to prevent bioresorption from occurring before tissue healing is accomplished. Uncontrolled or high corrosion rates in the physiological environment may result in the bioresorbable implant's early embrittlement and loss of structural integrity [14]. Technological solutions that enable reduction and control of degradation rates can favor a wider utilization of biodegradable temporary implants, avoiding concerns about metal fix implants [21,22].

Different approaches, such as alloy composition, surface modification, and conversion coatings, have been proposed to improve and to better control the corrosion kinetics of magnesium alloys [14,22–26]. Namely, ion implantation [27–29], organic coatings [30–33], alkali heat treatment, micro-arc oxidation [34–36], and polymer coating [37–39] have been proposed. Among these, biodegradable polymer coatings have been described to have better performance [40–42], even if not yet providing proper coating durability or good biocompatibility.

PHB (Poly-β-hydroxybutyrate) is a natural macromolecule polymer secreted by microorganisms under the condition of unbalanced growth that was chosen for our study as a biodegradable protecting and corrosion rate-controlling coating for magnesium alloy [32].

PHB and its copolymers are already used in a wide range of applications for drug release and tissue engineering, since it is naturally and not toxically biodegraded in CO_2 and H_2O by the human metabolism and does not cause body immune exclusion. Tissue response to PHB degradation byproducts is debated. Rat subcutaneous tissue reactions following implantation of PHB and PHB/VA have been reported [43] with the hypothesis that mononuclear giant cells infiltrate hyperplasia of fibroblasts, and mature fibrous capsules were a typical reaction associated with an increase in the collagen deposition induced by PHB degradation byproducts. However, in vivo tests run [44] using PHB films implanted subcutaneously in rabbits' legs for 8 weeks showed that the presence of macrophages was not accompanied by any acute inflammation or abscess formation. The experiment

suggested that PHB material has good biocompatibility and biodegradation [45] associated to good chemical and mechanical properties for biomedical applications [15,45–53].

In the present work, both the surface characterization and biological response of magnesium alloy AZ31 coated with poly-β-hydroxybutyrate (PHB) were evaluated to investigate whether it could induce low hemolysis and its effects on cell viability. Such experimental research provides a preliminary evaluation of magnesium alloys with PHB coating as vascular stents and hard tissue repair materials, and it will serve as a base and reference for their future potential clinical applications.

2. Materials and Methods

2.1. Materials

Magnesium AZ31 alloy extruded bars with chemical composition (wt.%) 2.89 Al, 0.92 Zn, 0.05 Mn, 0.01 Si, 0.002 Cu, 0.001 Ni, 0.004 Fe, and the complement 96.123 Mg were obtained from Guangdong Dongguan Hongxing Metal Materials co., LTD., Dongguan China. Reagent grade poly-β-hydroxybutyrate (PHB) was purchased from Santa Cruz Biotechnology, Santa Cruz CA, USA.

2.2. Preparation of Mg Alloy Disks and Coating Procedures

Specimens were cut from the AZ31 magnesium alloy bars. Small disks with dimensions 13 mm diameter and 2 mm thickness were obtained. Each sample was mechanically ground up with 1200-grit SiC paper, ultrasonically cleaned in acetone, and rinsed with ethanol and distilled water. PHB was dissolved in trichloromethane (analytical grade) at a concentration of 1 wt%. Organic PHB dip coating on Mg AZ31 alloy disk was carried out by a two-step process: first a 2 h hydrothermal treatment at 100 °C [43], the scope of which was to obtain an uniform surface for all samples with a homogeneous $Mg(OH)_2$ layer that favors polymer coating adhesion, was carried out followed by dip coating in the PHB solution with subsequent solvent evaporation at 20 °C for 24 h. Magnesium AZ31 alloy control specimens without polymer coating were also collected after the hydrothermal treatment. Polymer coating thickness was indirectly determined by gravimetric measurements of the samples before and after the coating procedure. Sample weight increase after solvent evaporation of the 1% polymer solution was rationally assumed to be due to the formation of a homogeneous thin polymer film covering the entire sample surface, the thickness of which was extrapolated considering the exposed surface area of the sample (3.47 cm^2) and PHB polymer density (1.25 g/cm^3). The gravimetric calculated mean coating thickness was 52 ± 6 μm.

2.3. Alloy Surface Morphological and Chemico-Physical Characterization

The surface morphology of the specimens was analyzed by scanning electron microscopy (SEM) (VegaIII-LMH, Tescan, Czech Republic). Molecular structure and chemical composition of the surface material were investigated by Fourier transform spectrum (FTIR). Sample wettability was determined by using a contact angle meter (Future Digital Scientific, Taiwan).

2.4. Electrochemical Analysis

Electrochemical measurements were performed by utilizing an electrochemical workstation (Chen Hua CH604B, Shanghai) with a three-electrode setup: the specimen as working electrode (1 cm^2 area exposed), a platinum sheet as counter-electrode, and a saturated calomel electrode (SCE) as reference electrode. Fifty milliliters of deoxygenated m-SBF incubated in a water bath at 37 ± 0.2 °C served as electrolyte. Potentio-dynamic polarization curves were scanned from −2 V to −1 V at a scan rate of 2 mV/s. The natural corrosion current (I_{corr}) and natural corrosion potential (E_{corr}) were determined by Tafel extrapolation.

2.5. Static Degradation Tests

The corrosion tests on reference and PHB-coated Magnesium AZ31 alloy were carried out at 37 °C in a simulated body fluid (SBF), the composition of which in mmol/L is reported in Table 1, following metal corrosion test standard ASTM-G31-72. Specifically, solution volume-to-sample area ratio should be between 20 mL/cm^2 and 40 mL/cm^2; in our test, the selected ratio was 30 mL/cm^2. Identical reference and coated samples were immersed in separate flasks containing the same corrosion fluid (SBF). We daily collected SBF solution samples to measure their pH values (by electrochemical pH meter) and magnesium ion concentration (by inductively coupled plasma-mass spectrometer) and as a culture medium to run the biological tests. After daily sampling, SBF solutions were renewed for all samples over the entire period of the corrosion tests (15 days). Uncoated and coated samples' individual measurements had four repetitions. At one-day time intervals, a group of PHB-coated and uncoated AZ31 disks was daily removed from the SBF, gently rinsed, and cleaned with 180–200 g/L chromium trioxide for 5–10 min and then air dried for individual gravimetric measure of their daily weight losses as a function of SBF exposure time.

Table 1. The concentration of inorganic ions in simulated body fluid (SBF) and blood plasma.

Ions	Plasma, mmol/L	SBF, mmol/L
Na^+	142.0	142.0
K^+	5.0	5.0
Mg^{2+}	1.5	1.5
Ca^{2+}	2.5	2.5
Cl^-	103.0	147.8
$(HCO_3)^-$	27.0	4.2
$(HPO_4)^{2-}$	1.0	1.0
$(SO_4)^{2-}$	0.5	0.5
pH	7.2–7.4	7.4

According to gravimetric measurements and inductively coupled plasma-mass spectrometry, corrosion rates were respectively evaluated as daily weight loss (mg/cm^2 per day) and daily released Mg^{2+} ion mass (mg/cm^2 per day). Moreover, following the ASTM-G31-72, corrosion rate was also evaluated as μm/day both from gravimetric and mass spectrometry measurements.

2.6. Cell Culture

HUVECs were cultured in endothelial basal media (RPMI 1640; HyClone, Cytiva, Saly Lake City, UT, USA) and Dulbecco's Modified Eagle Medium/F12 (DMEM/F12), respectively. Both were supplemented with 10% fetal bovine serum (FBS; Cambrex Corp, E.Rutheford, NJ, USA) and 1% antibiotic/antimycotics solution (Gibco Industries Inc., Langley, OK, USA). Cells were grown to confluence in T-75 culture flasks (Falcon, BD Biosciences, San Diego, CA, USA) at 37 °C under 5% CO_2.

2.7. Cytotoxicity Assessments

The effect of metal ions released from magnesium alloys was evaluated by using Cell Counting Kit-8 (CCK-8) (Beyotime Biotechnology, Shanghai, China) to determine the percentage of viable human umbilical vein endothelial cells (HUVECs) in extract solutions exposed to different concentrations. The cells were cultured in RPMI1640 media (Hyclone, USA), 10% fetal bovine serum, FBS (Gibco, USA), and Penicillin-Streptomycin at 37 °C in a humidified atmosphere with 5% CO_2. The AZ31 alloys were immersed in RPMI1640 media for 72 h (the ratio of the sample surface area and extraction medium using 1.25 cm^2/mL). The leaching solution was prepared at concentrations of 25%, 50%, and 100%. Cells were counted (2×10^4 cells) using a hemocytometer and plated in 96-well plates with 200 μL of culture media per well. The cells were incubated for 24 h to allow attachment. After the

24 h incubation, the culture media was replaced with culture media exposed to magnesium alloys. Pure culture media with cells was used as control. The cells were incubated for 24 h. After the 24 h, 100 µL of media were removed from the 96-well plates, and the remaining 100 µL media was treated with 20 µL/well CCK Solution Reagent. The 96-well plates were placed in the incubator for 4 h. After the incubation period, optical density measurements were recorded using an ELx800™ BioTek absorbance microplate reader controlled by Gen5 software with a 490 nm absorbance excitation filter.

2.8. Hemolysis Assessments

Healthy human blood from a volunteer containing sodium citrate (3.8 wt.%) in the ratio of 9:1 was taken and diluted with normal saline (4:5 ratio by volume). Samples were dipped in a 15 mL centrifuge tube containing 10 mL of normal saline that had been previously incubated at 37 °C for 30 min. Then, 0.2 mL of diluted blood was added to this standard tube, and the mixtures were incubated for 60 min at 37 °C. Similarly, normal saline solution was used as a blank control and deionized water as a positive control. After that, all the tubes were centrifuged for 5 min at 3000 rpm, and the supernatant was carefully removed and transferred to the 96-well plates for spectroscopic analysis at 545 nm.

The hemolysis, based on the average of three replicates, was evaluated by optical density (OD) measurements using an ultraviolet spectrophotometer (UNIC-7200, UNIC, Shanghai, China) according to Equation (1):

$$\text{Hemolysis} = (OD_{test} - OD_{negative\ control})/(OD_{positive\ control} - OD_{negative\ control}) \times 100\% \quad (1)$$

where OD_{test} stands for the optical density of the test group, $OD_{negative\ control}$ stands for that of the normal saline control group, and $OD_{positive\ control}$ stands for that of the deionized water group.

2.9. Nitric Oxide (NO) Assessments

Cells were counted (2×10^4 cells) using a hemocytometer and plated in 24-well plates with 500 µL of cell suspension per well. Pure culture media with cells was used as control. After 24 h, SBF corrosion extraction fluids at different dilutions were used to replace the original culture medium, and the supernatant was obtained after 24 h of culture. Experimental procedures were performed in accordance with a nitric oxide (NO) assay kit (Nanjing Jiancheng Bioengineering Institute, Nanjing China). The absorbance of each well was measured at 570 nm of the microplate reader.

2.10. Total Antioxidant Capacity (T-AOC) Assessments

Cells were counted (2×10^4 cells) using a hemocytometer and plated in 24-well plates with 1 mL of cell suspension per well. The following experimental procedures were performed in accordance with a total antioxidant capacity (T-AOC) assay kit (Nanjing Jiancheng Bioengineering Institute, China).

2.11. Statistical Analysis

Each experiment was repeated at least three times, and the data are expressed as the mean ± the standard deviation (SD). Comparisons among values for all groups were performed by one-way analysis of variance (ANOVA). Holm's *t*-test was used for analysis of differences between different groups. Differences were significant at $p < 0.05$.

3. Results

3.1. Morphological and Electrochemical Characterization of the Samples' Surfaces

Scanning electron micrographs of the surface morphologies of the uncoated and PHB-coated AZ31 samples are shown in Figure 1a–d.

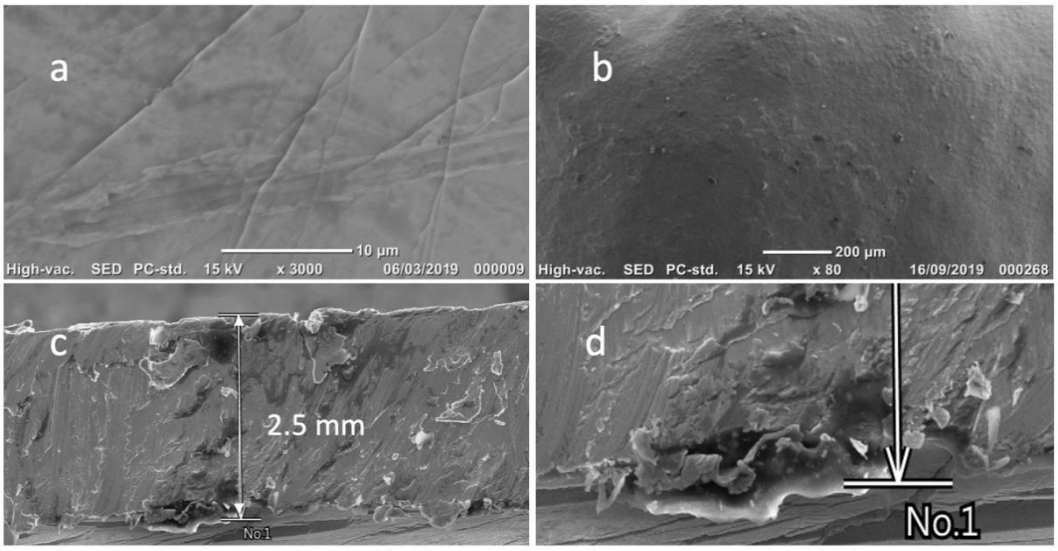

Figure 1. Characterization of the PHB coating. (**a**) Surface morphology of AZ31 and (**b**) AZ31 coated with PHB under the scanning electron microscope. (**c**) PHB-coated sample fractured section and (**d**) detail of the PHB coating.

The surface of the thermally treated AZ31 magnesium alloy exhibits a relatively smooth noncontinuous surface with snaking lines that were probably due to the formation of a nonhomogeneous magnesium hydroxide layer during the hydrothermal treatment. Conversely, PHB-coated samples are characterized by much more homogeneous surfaces (Figure 1b). Details of the fractured sample section are reported in Figure 1c,d, where it is possible to see the PHB surface-coating film.

From these images, it appears that the polymer film was uniformly distributed across the surface and that it well adhered to the hydrothermally treated metal surface. From the image of the section of the cold fractured coated samples (Figure 1c and, in detail, Figure 1d), both adhesive and cohesive failures of the polymeric coating are visible.

Direct measurements of the adhesion strength during our time testing were carried out; however, no evidence of PHB corrosion was microscopically noticed after the 2 weeks of the tests.

The molecular characteristics and chemical compositions of AZ31 and PHB-coated AZ31 sample surfaces were spectroscopically investigated. FTIR spectra are compared in Figure 2a,b.

The left FTIR spectrum, Figure 2a, which represents the uncoated alloy, shows the presence of an absorption band at 3343 cm^{-1}, which represents the existence of an (OH) bond possibly associated to a superficial layer of the magnesium hydroxides.

The surface absorption spectrum of the polymer coated samples, reported in Figure 1d, consistently with the standard spectrum of PHB, presents a 3437 cm^{-1} peak associated to the stretching vibration of hydroxyl OH; the 2978 cm^{-1} peak of the stretching of saturated CH; the 1725 cm^{-1} of the stretching of C = O; the 1456 cm^{-1} and 1381 cm^{-1} of CH_3- and -CH_2- deformation vibration; the 1291 cm^{-1}~1058 cm^{-1} PHB ester band; and, finally, the 826 cm^{-1} absorption peak of CH_2 groups.

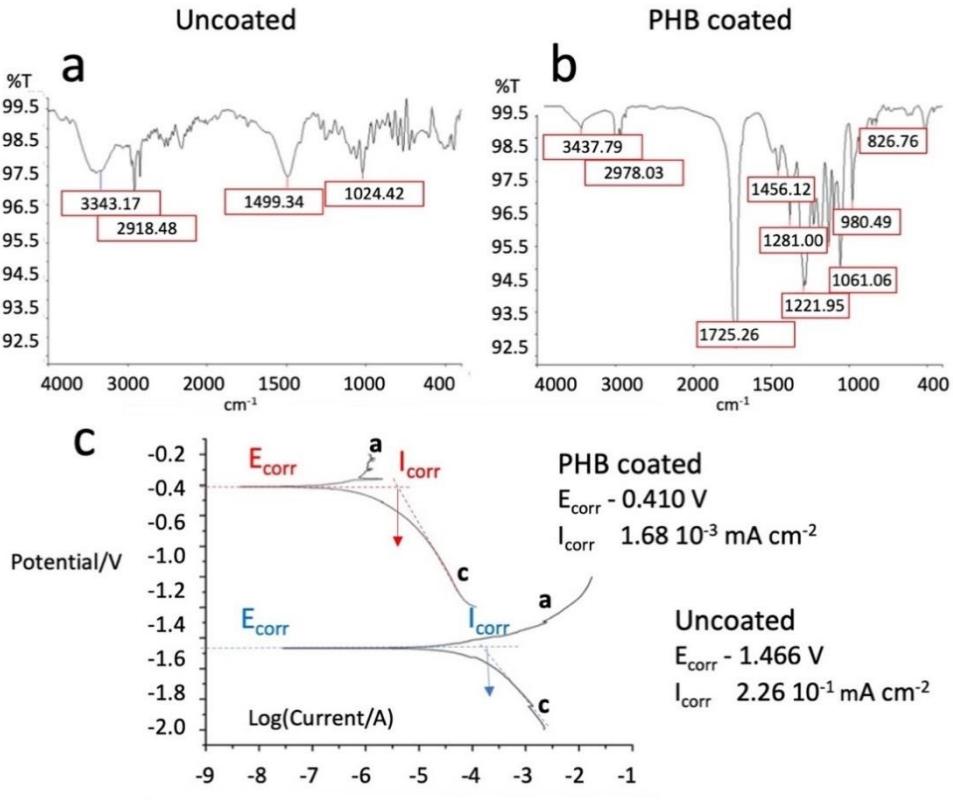

Figure 2. (**a**) FTIR spectra results of AZ31 and (**b**) AZ31 with PHB coating; (**c**) comparison of polarization curves and natural corrosion potential (E_{corr}) and current (I_{corr}) for PHB-coated and uncoated AZ31 Mg alloy.

These results confirm that the AZ31 alloy sample developed a magnesium hydroxide surface layer [43] after hot water treatment that was successively homogeneously covered by the thin film of PHB polymer.

Cathodic and anodic polarization plots are described in Figure 2c. The natural corrosion current (I_{corr}) and natural corrosion potential (E_{corr}) determined by Tafel extrapolation (dotted lines) for the PHB-coated and uncoated Mg alloys are also reported in Figure 2c.

The I_{corr} value for the PHB-coated sample is two orders of magnitude lower than that of the uncoated AZ31 alloy. Since I_{corr} is directly proportional to the corrosion rate [38], a drastic improvement in corrosion resistance is achieved by PHB coating that can be attributed to the hindering of the oxidation and reduction reactions occurring at the metal interface.

Magnesium corrosion in aqueous media first implicates reaction of H_2O with Mg to produce $Mg(OH)_2$ and H_2. The overall reaction comprises the anodic reaction $Mg \rightarrow Mg^{2+} + 2e^-$ and the cathodic reaction $2H_2O + 2e^- \rightarrow H_2 + 2OH^-$, which accounts for the increase of the solution pH [53–55]. After a hydrothermal passivation treatment (as was the case for our samples), the Mg AZ31 alloy surface was covered by a $Mg(OH)_2$ layer. During the polarization tests, metal cation transport controls the anodic Mg dissolution kinetic at the metal interface beneath the $Mg(OH)_2$ layer. The unstable in aqueous environment and porous layer cannot hinder electrolyte penetration and diffusive transport. Charge transfer associated with cathodic reactions can, then, freely occur both underneath and on top of this layer, which can collapse, increasing the charge transfer at advanced stages of the corrosion process.

The natural corrosion current of the uncoated alloy, which was significantly higher than that measured for PHB-coated samples, depends on this high charged species mobility. For the PHB-coated alloy, conversely, the exchange current density from the cathodic reaction is reduced because the more hydrophobic polymer film acts as a physical barrier that retards water penetration as well as electron and ion transport.

The abrupt deviation of the anodic branch (a) in the Tafel polarization plot of the PHB-coated sample could be attributed to the passivation of the anode surface. The anodic metal passivation and dissolution rate reduction occur as the PHB coating significantly slows the diffusive mass transport of anions and cations [56].

The formation of polar secondary PHB-Mg^{2+} bonds (due to the high number of oxygens present in the polymer structure) at the metal–polymer interface may further hinder anodic reactions [56]. The layer of PHB coating also retards bulk polymer anion diffusion from the SBF corroding medium to the metal interface, resulting in a final natural corrosion current about two orders of magnitude lower of that of the bare AZ31 sample.

The shift of natural corrosion potential of the PHB-coated alloy towards the anodic direction and its passivation indicates that the polymer film acts as a physical barrier that strongly hinders the electrolytes anions migration from the SBF corroding solution to the cathode [56].

These anodic and cathodic polarization plots are further discussed in next section in relation to their correlations to wettability and the SBF corrosion tests in terms of PHB diffusive barrier characteristics.

3.2. Wettability, Polarization Curves, and SBF Corrosion Tests

Surface wettability of AZ31 Mg alloy was investigated by contact angle measurements. Water contact angles are reported in Table 2 for *not hydrothermally treated* and *hydrothermally treated* samples with and without PHB coating.

Table 2. Water contact angles for AZ Mg alloy not hydrothermally treated (first column), hydrothermally treated with the formation of a $Mg(OH)_2$ surface coating (second column), and hydrothermally treated with an additional PHB coating (third column).

AZ31 Mg Alloy	AZ31 Mg Alloy + $Mg(OH)_2$	AZ31 Mg Alloy + $Mg(OH)_2$ + PHB
46.1° ±2.5°	* 42.2° ±0.4°	** 62.3° ±0.3°

* significant difference ($p < 0.05$); ** highly significant difference ($p < 0.01$).

The wettability tests confirmed the presence of a continuous surface layer of $Mg(OH)_2$ on the hydrothermally treated samples. As reported in Table 2, in fact, the not hydrothermally treated MG alloy showed significantly higher contact angle value and variance (46.1° and ±2.5° respectively) compared to those of the hydrothermally treated ones (42.2° and ±0.4°, respectively). It can be inferred, then, that the significantly lower data variance of the treated samples could be attributed to more homogeneous surface properties guaranteed by the formation of a homogeneous layer of $Mg(OH)_2$.

In particular, the contact angle of the not hydrothermally treated AZ31 alloy was about 46.1°, indicating a mild hydrophilic character. However, after the hydrothermal treatment, the measured contact angle lowered to 42.2°, indicating that the hydrothermally formed magnesium hydroxide increased the sample surface's hydrophilicity. Conversely, the presence of a PHB polymer coating on the hydrothermally treated AZ31 metal surface significantly increased the contact angle up to 62.3°, considerably lowering its wettability compared to that of the only hydrothermally treated one. The more hydrophobic the outer layer, the lower the surface wettability and the lower the water penetration rate [53–55].

Surface wettability, then, could play a relevant role in the corrosion and biological responses of implanted devices because it influences water and solution electrolyte diffusion, the chemistry of corrosion, protein absorption, and cell activity at the implant interface. This could be particularly significant in the case of magnesium alloy prostheses. When implanted in the body, the magnesium alloy is in contact with body fluids that wet its surface, starting a corrosion and resorption process that may become detrimental to its functionality if it occurs at too high rates [57].

Our wettability test indicates that the presence of a $Mg(OH)_2$ layer increases magnesium alloy wettability and, therefore, any associated detrimental effects, while the use of

the PHB coating, which significantly reduces surface wettability and protects the metal surface, could allow for better control of erosion processes, lengthening its functionality.

From the previous discussion, it can be inferred that for implanted prostheses, magnesium erosion and ion release in the biological surrounding environment could be directly related to the electrochemical character of the reduction and oxidation reactions occurring at the metal interface and the external electrolytic solution.

Information on the corrosion rate, passivity, pitting susceptibility, and cathodic and anodic behavior of an electrochemical system can be obtained by interpreting the polarization curves reported in Figure 2c for bare and PHB-coated Mg alloy.

The magnitudes of the natural corrosion current I_{corr} and natural corrosion potential E_{corr} act as driving forces dictating the type and rates of anodic and cathodic electrochemical processes that could take place at the metal–corroding solution interface.

It is generally agreed that the larger the corrosion current density, the higher the corrosion rate, that is, the lower the corrosion resistance of the metal [53,54].

The results of the 15-day SBF corrosion test on PHB-coated and uncoated Mg AZ31 alloy carried out according to the ASTM-G31-72 are reported in Figure 3. In particular, the pH change of the SBF corroding medium, the mass of the Mg^{2+} corrosion ions released in the SBF, and the gravimetric samples' weight losses were recorded each day before solution refreshing and are reported in Figure 3a–c, respectively. The curves interpolating the experimental data reported in Figure 3 were obtained by mobile mean curve fitting with a period of two.

The PHB-coated Mg AZ31 samples clearly exhibited in all three diagrams a significantly different corrosion behavior compared to that of the uncoated system.

At the end of each exposure day, the initial pH value of the corroding medium rose from 7.4 to values steadily ranging from 7.6 to 7.8 over the entire 15-day test for the PHB-coated metal samples (red curve in Figure 3a), while that of the uncoated alloy (blue curve in Figure 3a) presented a more scattered distribution and a higher basic character with pH values risen to 8.0–9.5. For all the uncoated samples tested, an abrupt increase of pH after day 9–10 of the corrosion test was observed. This event could be attributed to the previously described porous $Mg(OH)_2$ layer collapsing due to the corrosion reactions and Mg^{2+} ion ablation from the metal–hydroxide interface [52,53].

Magnesium, when exposed to aqueous environments, develops a superficial porous hydroxide film that only moderately protects the metal from external aggressive liquid environments, thus only partially hindering and slowing down any potential corrosion process [56,57]. However, $Mg(OH)_2$, although only slightly soluble in water, undergoes severe modifications in presence of chloride ions, which could occur in the case of use in contact with physiological solutions.

$Mg(OH)_2$, reacting with Cl^-, forms the highly soluble $MgCl_2$ and molecular hydrogen [57]. This continuous dissolution process is accompanied by a progressive increase of the corroding medium basicity (as we have observed in our corrosion tests reported in Figure 3a). In these conditions, pitting of magnesium and embrittlement of the $Mg(OH)_2$ layer could occur at advanced stages of the corrosion process.

The abrupt pH increase at days 9–10 can thus be associated to the collapse of the magnesium hydroxide layer, which caused the direct exposure of the metal surface to the corroding medium. This occurrence, consistently with our experimental data, i.e., observed daily released Mg^{2+} ions (reported in Figure 3b as mg per sample cm^2) and daily gravimetrically measured sample weight losses (reported in Figure 3c as mg per sample cm^2), led to an increase of Mg^{2+} ion concentration in the corroding medium and to a massive sample weight loss.

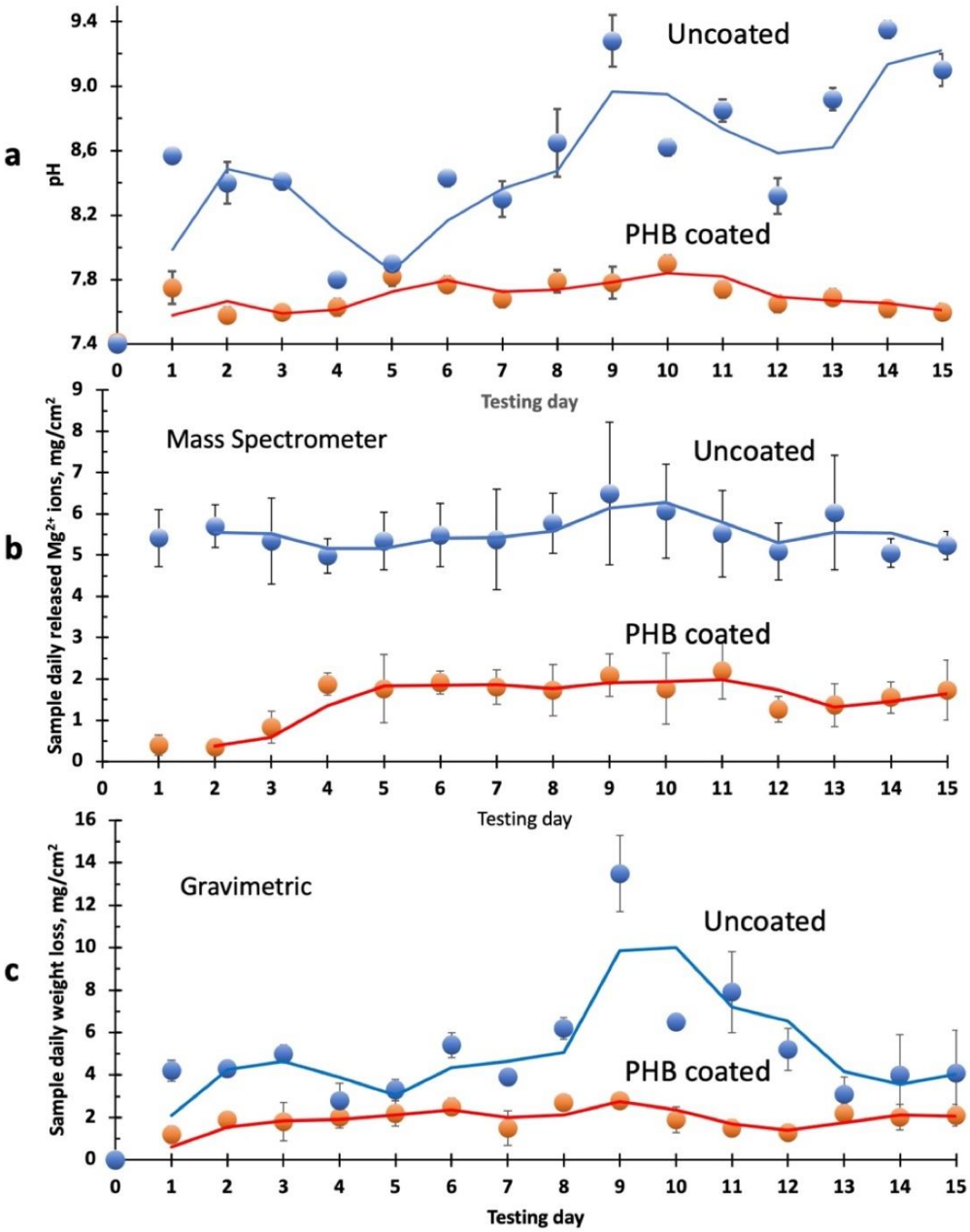

Figure 3. (**a**) pH of the SBF corroding medium, (**b**) mass of Mg^{2+} corrosion ions released in the SBF, and (**c**) gravimetric sample weight losses. Test were run according to ASTM-G31-72; SBF corroding medium was daily refreshed.

The mass of Mg^{2+} released from the uncoated magnesium alloy, in fact, was observed to be constantly higher than that from the PHB-coated ones. This higher tendency to release Mg^{2+} ions is consistent with the previously described measurements of anodic and cathodic polarization curves and values of the natural corrosion current reported in Figure 2c; the natural corrosion current I_{corr} of AZ31 coated with PHB was, in fact, two orders of magnitude lower than that of the uncoated alloy (1.68×10^{-3} mA cm^{-2} vs. 2.26×10^{-1} mA cm^{-2}).

The electrochemical observations confirm the hypothesized corrosion mechanism of the SBF immersion corrosion tests, where a higher diffusion resistance and lower cation and anion mobility are induced by the PHB coating in AZ31 Mg alloy.

It can be supposed, then, that the degradation rate of the AZ31 coated with PHB was significantly reduced by the presence of the polymeric coating film, which acted as a

membrane steadily controlling the diffusion flux of the ionic species (especially Cl^- anions) from the SBF solution to the metal surface and the counterdiffusion of Mg^{2+} metal ions toward the external solution. Conversely, the mere presence of the less stable (especially in presence of chloride ions) porous magnesium hydroxide layer cannot equally guarantee constant and effective corrosion control.

The hypothesized diffusive nature of the control exerted by the PHB membrane protecting the metal can be confirmed by the experimental data in Figure 4, where the cumulative amount of Mg^{2+} ions released in the daily refreshed SBF corroding solutions (data reported in Figure 3b) is plotted as a function of the test time for PHB-coated and uncoated Mg AZ31 alloys.

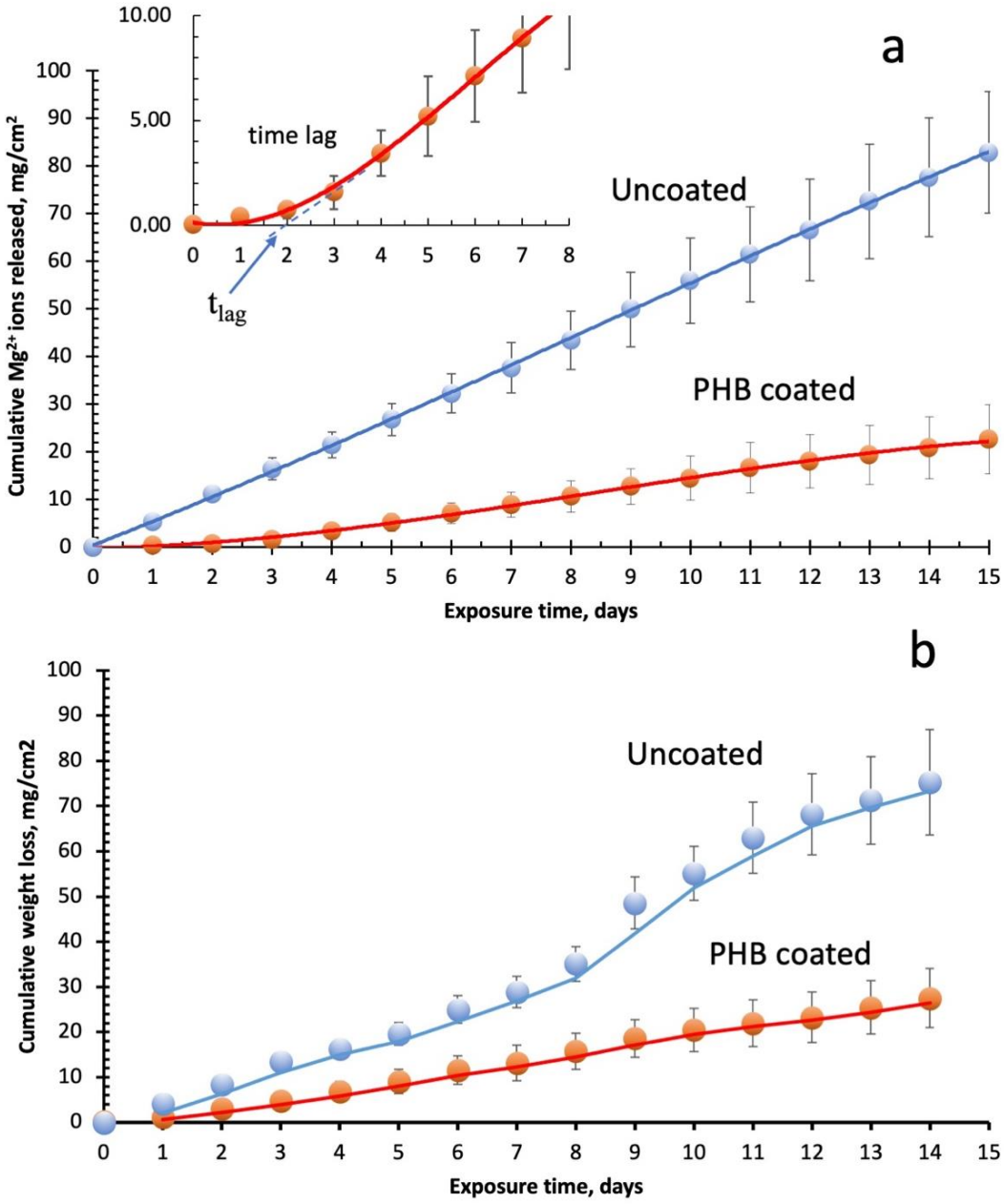

Figure 4. Cumulative Mg ion release (**a**) and weight loss (**b**) kinetics during corrosion tests. Details of the initial kinetic and time lag in the upper left part of the figure.

A steady state constant flux of Mg corrosion ions for the uncoated system (blue line in Figure 4) can be observed from the early stages of the test, while a *time lag* before reaching stationary flux is observed for the PHB-coated system. A detail of the initial part of the Mg ions release curve is reported in the upper-left corner of Figure 4. The upward shape of the Mg ion release curve before reaching a steady, constant slope is a characteristic observed in permeability tests due to the initial diffusion and sorption of the solution components in the still unpenetrated polymer.

In presence of the PHB membrane, a diffusive control is exerted on electrolyte mobility before steady state conditions of ionic species flux can be reached. This diffusive resistance (time lag) in our tests can be evaluated from the intercept on the time scale (t_{lag}) of the linear part of the curve, namely, 1.9 days. Corrosion rates can be directly evaluated for PHB-coated and uncoated alloys from the slopes of the curves at their stationary conditions. The corrosion rate for the PHB-coated Mg alloy was almost four times slower than that of the uncoated system at 1.25 and 5.5 mg/cm^{2}day, respectively (which, according to ASTM-G31-72, correspond to respective metal corrosion rates of 7.2 and 31.6 µm/day).

Permeability test and time lag measurements in permeation tests have been proven [58,59] to be effective methods to characterize permeability and diffusion coefficients of dissolved species. In the case of the corrosion test, the driving force for diffusion was the difference in concentration of Mg^{2+} ions between the metal interface, where they are steadily generated by corrosion reactions, and the corroding solution, which is maintained at a low Mg^{2+} concentration guaranteed by the daily solution refreshments.

Due to the simple nature of the permeation experiment, it can be schematized in our case that diffusive resistance can be directly obtained from experimental transient data preceding steady state permeation (time lag). The diffusion coefficient of Mg^{2+} ions in the PHB protective membrane can be evaluated using the standard time lag equation [58,59]:

$$D_{Mg}{}^{2+} = l^2/6\, t_{lag} \quad (2)$$

where t_{lag} is the time lag (1.9 days), l is the membrane thickness ($5.2 \pm 0.6 \times 10^{-3}$ cm), and $D_{Mg}{}^{2+}$ is the resulting diffusion coefficient, which in our testing condition is $2.7 \pm 0.5 \times 10^{-11}$ cm^2/s. This Mg^{2+} ion diffusion coefficient, which accounts for the mutual cation and anion self-diffusion coefficients $D+$ and $D-$ and solubilities in the polymer, is coherent with the values observed for highly crystalline and hydrophobic polymers [60] such is PHB polymer. Due to the charge neutrality, the Mg^{2+} cation diffusion in the PHB bulk coating toward the external SBF solution is also dependent on the counterdiffusion of the anionic species (especially the Cl^- ions that are directly involved in the metal corrosion process). As previously emphasized when analyzing the potentiometric polarization curves of the electrochemical characterization, the very low natural corrosion current and the shift of natural corrosion potential of the PHB-coated alloy towards the anodic direction indicate that the polymer film principally acts as a physical barrier that strongly hinders electrolyte anion migration from the external SBF corroding solution to the metal.

3.3. Cytotoxicity (CCK-8 Assay)

Application of an indirect method provided experimental assessments for the biocompatibility assays. Potential detrimental effects on host cells of Mg alloy materials and treatments were tested in vitro using the international standards ISO-10993-5 and ISO-10993-12, which are commonly used to evaluate Magnesium alloys [45–53].

The SBF corrosion test solutions (which we will name "extraction fluids") of the PHB-coated and uncoated AZ31 alloy samples, which contained the corrosion byproducts after 1 day of exposure, were used to perform cytotoxicity trials at different dilutions, namely, 25%, 50%, and 100% of the initial concentrated extracted medium.

HUVEC viability in these two types of extraction fluids at different dilutions after 1 day, 3 days, and 5 days, respectively, is summarized in Figure 5 as percentage of viability in standard control fluid (RPMI1640 medium).

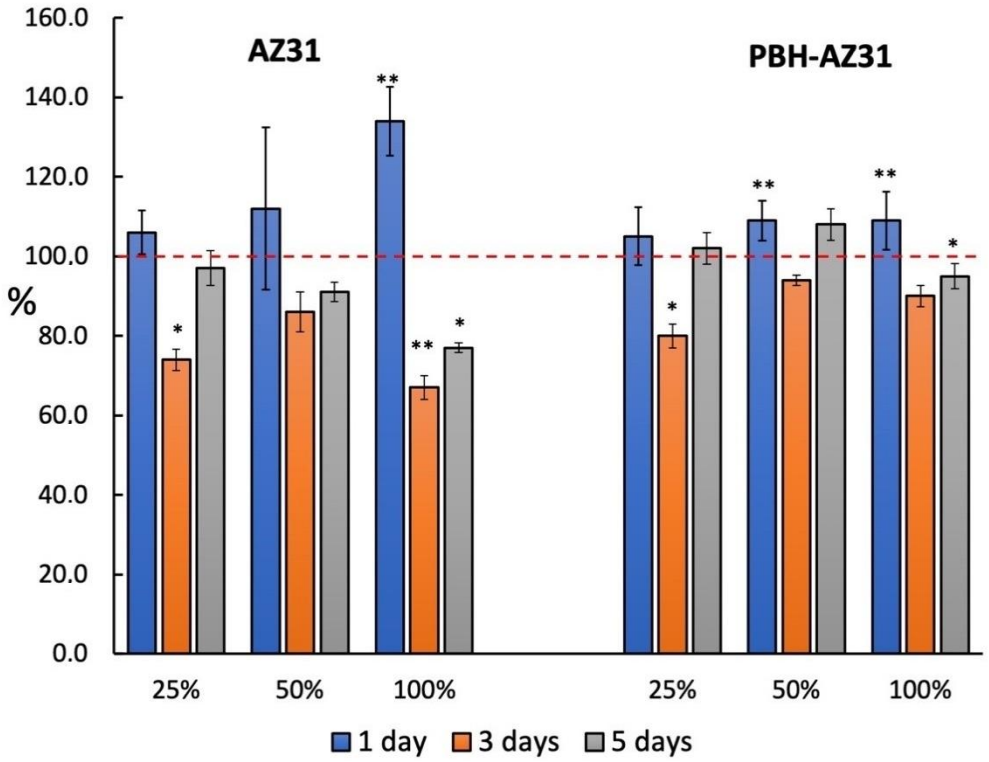

Figure 5. Proliferation of HUVECs cultured on extraction fluids after 1, 3, and 5 days. Data are reported as % of viability in standard control fluid. * Significant difference ($p < 0.05$); ** highly significant difference ($p < 0.01$).

After 1 day of exposure, significant, high differences in cell proliferations compared with the control were observed for 100% AZ31 extraction fluid and its 50% dilution, and for exposure to the 100% PHB-AZ31 extraction fluid. No significant differences with the control were observed for the other groups.

After 3 days of culture, significant differences for cell proliferation compared to the control were observed in 100% AZ31 extract fluid, in its 25% dilution, and in the 25% dilution of the PHB-AZ31 extraction fluid.

Finally, after 5 days of culture, only the 100% AZ31 extraction fluid had a significant effect on cell proliferation, while there were no significant differences between the other groups and the control.

It can be inferred that many favorable and adverse factors jointly influenced cell viability. The presence of Mg ions is one of these factors; it can act positively at lower concentrations (day 1), while cell growth adverse factors may arise at higher Mg ion concentrations (day 5). This point is to be further considered in future investigations.

The extraction fluid of the PHB-coated magnesium alloy, which was characterized by a significantly lower Mg ion concentration (see Figure 3b) had a significant effect on cell proliferation only in the early stage of the culture (1 day).

Table 3 includes the details of the relative growth rate (RGR) and cytotoxicity levels for the AZ31 and PHB-coated AZ31 extraction fluids and their dilutions. Levels of cytotoxicity were grade 0 for all extraction fluids and their dilutions when cultured for 1 day. After 3 days of culture, two of the three concentrations (25 and 100%) of the AZ31 extraction fluid exhibited a cytotoxicity level of grade 2, while the 50% was grade 1; all cytotoxicity levels for the PHB-coated samples were of grade 1. After 5 days of cell culture, the cytotoxicity

levels of the AZ31 sample fluids were all of grade 1, while two concentrations (25 and 50%) of the PHB-coated sample fluids showed a cytotoxicity of grade 0 and the other of grade 1.

Table 3. Cytotoxicity (CCK-8 assay) test details.

		Cultured 1 Day			Cultured 3 Days			Cultured 5 Days		
Extraction Fluid	**Conc. %**	**OD**	**RGR (%)**	**Toxic Grade**	**OD**	**RGR (%)**	**Toxic Grade**	**OD**	**RGR (%)**	**Toxic Grade**
AZ31	25	0.229 ±0.012	106	0	0.220 ±0.008	74	2	0.242 ±0.011	97	1
	50	0.243 ±0.045	112	0	0.255 ±0.015	86	1	0.227 ±0.006	91	1
	100	0.291 ±0.019	134	0	0.198 ±0.009	67	2	0.192 ±0.003	77	1
PHB-Coated AZ31	25	0.228 ±0.016	105	0	0.239 ±0.009	80	1	0.255 ±0.010	102	0
	50	0.254 ±0.011	109	0	0.280 ±0.004	94	1	0.269 ±0.010	108	0
	100	0.236 ±0.016	109	0	0.268 ±0.008	90	1	0.237 ±0.008	95	1

It can be noticed that the PHB-coated AZ31 magnesium alloy extraction fluid has a less toxic behavior and the capacity to promote cell proliferation. This peculiar behavior derives from the lower concentration of corrosion Mg^{2+} ions that directly originates from the diffusion control exerted by the polymeric coating films on the fluxes of the dissolved ionic species (both from the metal surface to the solution and *vice versa*).

3.4. Hemolysis

As previously discussed, the PHB polymer coating significantly reduced the Mg AZ31 alloy corrosion rate in SBF and reduced the concentration of corrosion byproducts in the corroding medium.

Table 4 reports the optical density measurements utilized for the evaluation of the hemolysis ratio from the spectroscopic analysis of incubated extraction fluids of magnesium alloy with and without PHB polymer coating with diluted blood and the positive and negative controls. In the last column is reported the Mg^{2+} concentration of the respective extraction fluids after 72 h of PHB-coated and bare alloy sample conditioning.

Table 4. Detailed data of hemolysis rate testing.

Sample	OD Value	Hemolysis Rate	Mg^{2+}, mmol/L
AZ31 Mg	0.2487 ± 0.0775	37.61%	22.9 ± 1.3
PHB-coated AZ31 Mg	0.0530 ± 0.0117	4.19%	2.4 ± 0.2
Positive control	0.6137 ± 0.0117		
Negative control	0.0285 ± 0.0117		

The results indicate that the corrosion medium of the bare uncoated magnesium alloy induces a serious hemolysis process, with a rate that was as high as 37.61%, compared to that of the PHB-coated alloy samples, where the hemolysis rate was 4.19%, showing better blood compatibility and meeting the requirements for application as medical material (5%).

The concentration of magnesium ions has a great influence on blood as well as on tissue cells. An AZ31 magnesium alloy implanted in the body, if characterized by a too high degradation rate, will lead to an excessive and dangerous increase of magnesium ion concentration in the fluid surrounding the implant with a detrimental effect on patient health.

After 72 h SBF conditioning, the content of Mg^{2+} ions in the bare magnesium alloy corrosion fluid was as high as 22.9 ± 1.3 mmol/L, while that of the PHB-coated alloy

corrosion fluid was only 2.4 ± 0.2 mmol/L, which remains in the range of variability of physiological fluids.

This result is in line with the hemolysis results discussed before. The too high Mg^{2+} ion concentration resulted in an increase of hemolysis that is to be attributed to the significant increase of solution ionic strength [53,54]. As Mg^{2+} ion concentration increases, the osmotic pressure of the solution rises. The osmotic differential can cause erythrocyte swelling and cell membrane rupture with release of free hemoglobin and consequent hemolysis of red blood cells.

3.5. NO Assay

Vascular endothelial cells are directly related to angiogenesis, and nitric oxide (NO) which is an important regulatory signal of angiogenesis. In Figure 6 are reported the absorbance values of NO during the test time. The results indicate that there was no difference between each group. We think the reason for this may be that the NO signal pathway is not closely related with the content of magnesium ions. Each group showed a better NO release compared with the normal group. This indicates that the magnesium alloy material is appropriate for NO release.

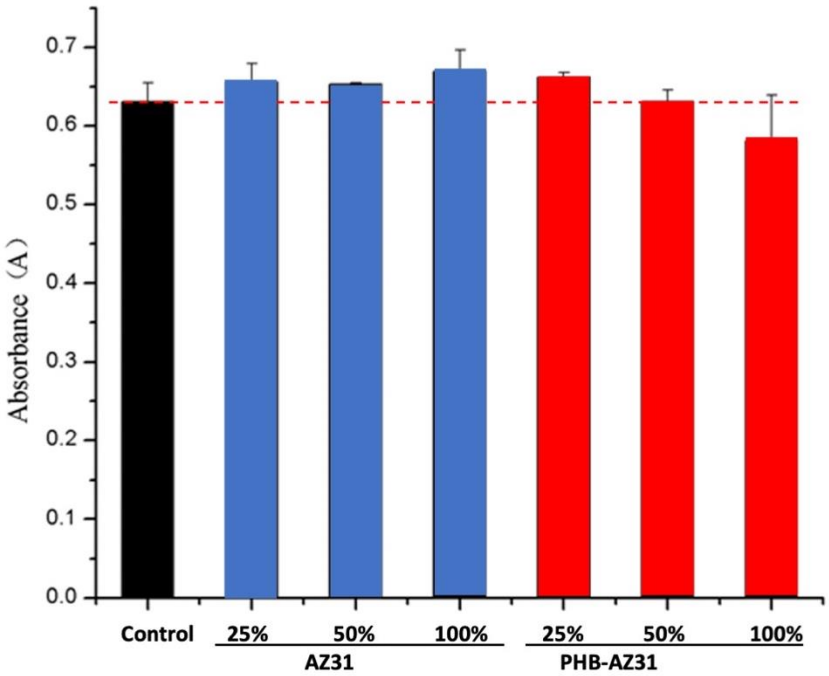

Figure 6. Nitric oxide (NO) absorbance results of the different groups.

3.6. T-AOC Assay

The normal physiological metabolism process of biological tissue can produce reactive oxygen species, and some environmental factors, such as ultraviolet radiation, γ-ray irradiation, environmental pollution, and other factors, can also induce the production of reactive oxygen species. Producing reactive oxygen species can lead to intracellular lipid, protein, and DNA oxidative damage, therefore inducing oxidative stress and then causing tumors, atherosclerosis, rheumatoid arthritis, diabetes, liver damage, etc. For these reasons, it is particularly necessary to detect the total antioxidant capacity of the cells.

Figure 7 shows the results of the total antioxidant capacity assay. In general, the overall antioxidant capacity of the magnesium alloy with PHB surface coating was significantly higher than that of the normal group, and the total antioxidant capacity was significantly improved, indicating that the magnesium alloy material induced a very good enhancement on the total oxidation capacity of cells.

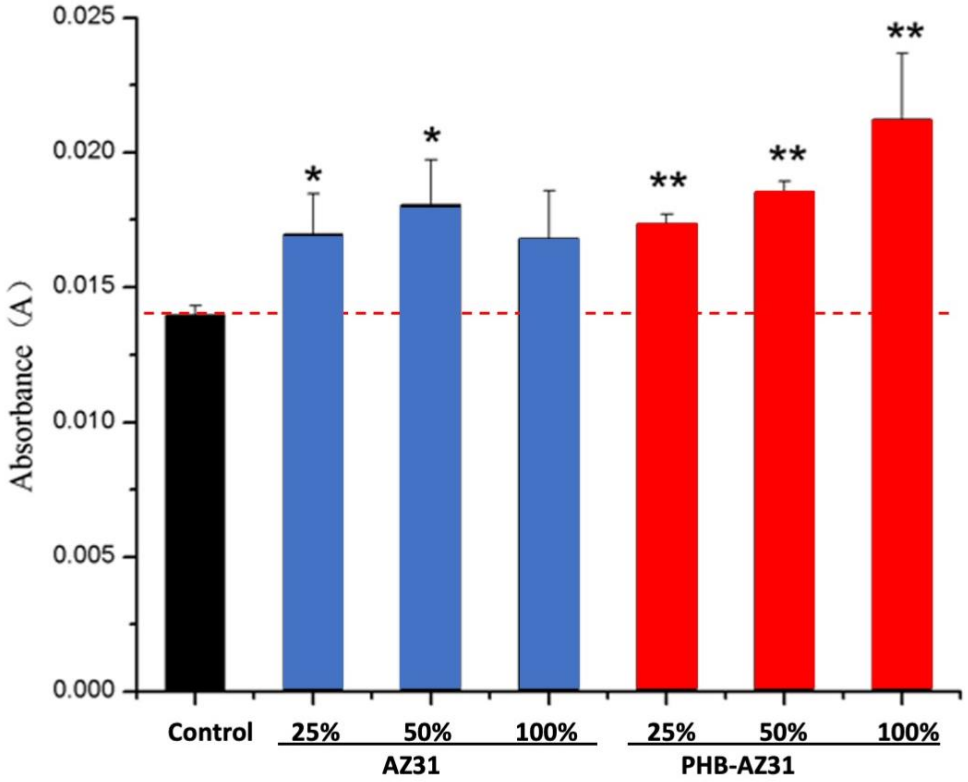

Figure 7. Total antioxidant capacity (T-AOC) contents of different groups. * significant difference ($p < 0.05$); ** highly significant difference ($p < 0.01$).

4. Discussion

The polymer coating was prepared by the PHB dip-coating method, while a magnesium hydroxide film, as confirmed by FTIR spectra, was formed on the alloy metal surface by hydrothermal treatment. The hydroxyl of magnesium hydroxide promoted the formation of hydrogen bonds with the PHB hydroxyls, improving adhesion strength between the polymer coating and the magnesium alloy surface. The corrosion natural current of uncoated magnesium AZ31 alloy was two orders of magnitude higher than that of the PHB-coated one, demonstrating that charge transport was drastically reduced by the presence of the polymeric coating.

It can be inferred that the reduced degradation rate of the AZ31 PHB-coated system is to be associated to the presence of the polymeric coating film, which acts as a membrane steadily controlling the diffusion flux of the ionic species (especially Cl^- ions) from the SBF solution to the metal surface and the counter-diffusion of Mg^{2+} metal ions toward the external solution. The results of static corrosion experiments on PHB-coated and uncoated AZ31 samples showed that under the same experimental conditions, weight losses were drastically reduced by the presence of the polymer coating, and Mg ion concentration and the pH value of the corrosion SBF medium were lower than those of the uncoated AZ31. The corrosion rate for the PHB-coated Mg alloy was more stable and almost four times slower than that of the uncoated system at 1.25 and 5.5 mg/cm^{2}day, respectively, which, according to ASTM-G31-72, correspond to surface ablation rates of 7.2 and 31.6 µm/day, respectively.

These findings showed that the polymer coating can not only significantly enhance the corrosion resistance of magnesium alloy materials but, due to the diffusive nature of the processes that driving the corrosion, it can also be used to program targeted resorption times. Control of resorption rates after implantation of and, hence, of Mg^{2+} ion concentration in body fluids could enlarge the field of application of these systems.

However, after implantation in the human body, a metal prosthesis's biocompatibility must fulfill a complex chain process [48–50]. First, blood and cell biocompatibility must be

evaluated. The hemolysis rate of PHB-AZ31 was lower than 5%, meeting the requirements of medical materials. Conversely, the hemolysis rate of bare AZ31 was 37.61%, which might induce more severe hemolytic phenomena because of the higher dissolution of magnesium ions of the uncoated AZ31. When red blood cells contacted with materials, a hemolysis phenomenon appeared because of the different osmotic pressures on both sides of the cell walls [51]. The hemolysis rate test proved that coated magnesium alloy materials showed good blood compatibility. Cell compatibility tests were also investigated; the results showed that corrosion extraction fluids with different concentrations infected endothelial cells differently. The higher extract concentration of the uncoated AZ31 induced greater endothelial injuries. The PHB-AZ31 extracts had no significant detrimental effect on cell proliferation because of the protection and diffusive control exerted by the polymer coating film, which maintained low, physiological levels of Mg^{2+} ions concentrations.

Cellular compatibility evaluation plays an important role in the evaluation of biological materials [52]. According to CCK-8 kit testing, PHB as a protective layer promoted cell proliferation. Angiogenesis means the formation of vascular lumen structures by endothelial cell proliferation and a migration process based on the existing network of blood vessels. Vascular endothelial cells are directly related to angiogenesis. On the other hand, NO is one of the most important control signals of angiogenesis. Before and after coating, NO content was not affected. Biological tissues can produce reactive oxygen species during normal physiological processes; in addition, some environmental factors, such as ultraviolet radiation, gamma radiation, and environmental pollution, can induce production of reactive oxygen species. When the reactive oxygen species is generated, it can lead to oxidation damage to cell lipids, protein, and DNA. Once oxidative stress is induced, it in turn leads to the occurrence of a variety of tumors, atherosclerosis, rheumatoid, nervous system diseases, etc. Therefore, T-AOC detection of cells is particularly necessary. Compared with normal groups, the T-AOC of PBH-AZ31 had significant enhancement.

Compared to other Mg alloys currently used as bioresorbable implant materials (such as ZX00, which contains 0.45% of Zn, 0.45% of Ca, and WE43, a rare earth Mg alloy containing up to 9% of yttrium, zirconium, and rare earth elements), AZ31 and PHB-AZ31 have been described to present improved corrosion resistance. Higher corrosion rates were observed [61] for rare-earth and lean Mg alloys compared to the AZ type; current–voltage curves and electrochemical impedance measurements confirmed that, for all Mg alloys, intermetallic particles acted as local cathodes; and more protective films were formed on the alloys' surface compared with pure Mg. The higher the presence of such intermetallic particles, the higher the corrosion resistance of the alloy. Mechanical, degradation, and osseointegration properties and the bone–implant interface strength of the AZ31 bioabsorbable magnesium alloy have been recently investigated [62,63].

Despite the promising biocompatibility performance of ZX00 for bone-implant applications, these Mg alloys still need an investigation of the materials' mechanical performance, and no information on alloys' ability of fracture stabilization or load-bearing efficiency is available. To further make these materials suitable for deployment in osteosynthesis, adequate stability during fracture healing must be guaranteed [64].

Poly-hydroxy-alkanoates (PHAs), bio-polyesters such as PHB synthesized by many bacteria, have been produced in large quantities for several research fields, including medical applications [65]. It has been demonstrated by many studies that PHAs possess the required mechanical, biodegradable, and tissue-compatible properties for implant applications. PHAs' biodegradation by products such as oligomers and monomers has been verified to be nontoxic to cells and tissues. Mechanisms of PHA bioactivity for cell growth have also been described [66]. PHAs have been therefore largely demonstrated as suitable bioactive matrices to support bone tissue growth and attachment and proliferation of bone marrow cells. These cells on PHB scaffolds, in fact, have been described to present typical osteoblast phenotypes such as round cell shape, high alkaline phosphatase activity, strong calcium deposition, and fibrillar collagen synthesis, indicating that PHBs are suitable biomaterial for bone tissue regenerations from bone marrow cells [67].

Literature on biodegradation indicated that the degradation of Polyalkenoates (such as PHB) may be targeted to occur in controlled time spans from few weeks to one year depending on blend or copolymer composition and that it is accelerated by the presence of enzymes [68].

Although not investigated in our paper, the effect of alloying elements (comprising Al, Mn, Cu, and Ni) on biodegradability and biocompatibility is described in literature on dissolved immersion media testing for cytotoxicity, hemolysis, and platelet adhesion [69]. The results showed that none of the tested alloying elements appreciably impaired the viability of vascular smooth muscle cells except for Mn, which increased the viability of the ECV304 cell line. The hemolysis percentage of these Mg alloys was less than 5%, and no sign of thrombogenicity was observed [70].

These investigations showed that the AZ31 alloy, although containing low percentages of Al and Ni that could induce some allergic reactions, associated with PHB (or other PHA) coatings may represent a promising material and a good compromise among biocompatibility, mechanical properties, and corrosion resistance, making this system tunable according to the timing of the specific application according to the corrosion properties required for the resorbable implant.

5. Conclusions

The scope of the present paper was initially addressed to understand the corrosion mechanism and to evaluate by biocompatibility tests the possibility using such system as a targetable viable system for bioresorbable implants.

The major drawback of using magnesium and its alloys in many engineering applications is its low corrosion resistance, especially when exposed to aqueous electrolytic environments. However, this characteristic may become an intriguing property for biomedical applications, where the in vivo corrosion of the magnesium-based implant, if adequately controlled, involves the formation of a soluble, nontoxic oxide and Mg ions that are harmlessly and easily excreted in urine. In addition, due to its functional roles and presence in bone tissue, magnesium may have stimulatory effects on the growth of new bone tissue [27–30].

Thus, it is predictable that magnesium and its alloys could be applied as lightweight, degradable, load-bearing orthopedic implants, which would remain present in the body and maintain mechanical integrity over a planned, controlled time scale while the bone tissue heals, eventually being replaced by natural tissue using biomechanical approaches [31,32,71,72]. The unfortunate complication is that pure magnesium can corrode too quickly in the physiological pH (7.4–7.6) and the high-chloride environment of the physiological system; polymer PHB was therefore investigated in our study as a potential magnesium alloy corrosion-controlling coating. SEM analysis showed that the morphology of the AZ31 magnesium alloy was changed, depicting smooth and flat features formed after PHB coating treatment. FTIR spectra confirmed the molecular and chemical composition for AZ31 and AZ31 coated with PHB. It indicated that AZ31 indeed formed a magnesium hydroxide layer on its exposed surface after hot water treatment. Wettability studies confirmed that PHB coating made the surfaces less hydrophilic. Static degradation and electrochemical experiments demonstrated that the corrosion rate decreased for PHB-coated AZ31 as compared to untreated surfaces. The corrosion controlling ability can be related to resistance to corroding molecules' diffusion to the metal surface, and to Mg ions' counter-diffusion to the solution, exerted by the polymeric film. The degradation rate can be then further reduced by increasing the polymeric film thickness and, hence, the diffusive hindering. This feature can allow specifically tailoring the coating thicknesses for different specific resorbable prosthetic applications.

In vitro analysis by indirect MTS assay showed that the experimental group may promote the proliferation of cells due to the presence and control of the PHB polymer coating. The hemolysis rate of the material indicated that PHB coating was indeed effective to slow down the degradation rate of magnesium alloy. Finally, NO and T-AOC analysis displayed PHB coating showed good biocompatibility.

This demonstrates that the PHB polymer coating can effectively avoid, in a potential clinical application of this Mg alloy, the detrimental effect of an intense and uncontrolled release in the body of Mg ions by reducing the metal degradation rate (which was evaluated. from the corrosion tests reported in Figure 4a. to be four times slower than that of the bare uncoated Mg alloy at 1.25 vs. 5.5 mg/cm^{2}day) and hence reducing the concentration of magnesium ions around this potential resorbable implant. Moreover, due to the diffusive nature of the control exerted by the polymer coating, corrosion rates may be programmed to specific times and levels of Mg ion concentration by properly modifying the coating thickness.

Author Contributions: Conceptualization, G.W. and A.A.; methodology, D.A., S.L., L.W., R.A., and V.P.; validation, Z.H., J.T., L.C., and S.G.; formal analysis, A.A. and Y.C.; writing—original draft preparation, G.W. and A.A.; writing—review and editing, A.A.; visualization, R.A. and A.A.; supervision, G.W. and A.A.; funding acquisition, A.A., G.W. All authors have read and agreed to the published version of the manuscript.

Funding: This study was partially supported by grants from the National Key Technology R&D Program of China (2016YFC1102305), the National Natural Science Foundation of China (31971242), the Visiting Scholar Foundation of Key Laboratory of Biorheological Science and Technology (Chongqing University), the Ministry of Education (CQKLBST-2016-001), the Chongqing Research Program of Basic Research and Frontier Technology (cstc2019jcyj-zdxmX0028), Fundamental Research Funds for the Central Universities (2021CDJCGJ007, 2019CDYGB016), and the Public Experiment Center of State Bioindustrial Base (Chongqing), China.

Institutional Review Board Statement: Not applicable.

Conflicts of Interest: The authors declare no conflict of interest.

References

1. Hou, Z.; Yan, W.; Li, T.; Wu, W.; Cui, Y.; Zhang, X.; Chen, Y.-P.; Yin, T.; Qiu, J.; Wang, G. Lactic acid-mediated endothelial to mesenchymal transition through TGF-β1 contributes to in-stent stenosis in poly-L-lactic acid stent. *Int. J. Biol. Macromol.* **2020**, *155*, 1589–1598. [CrossRef] [PubMed]
2. Lin, S.; Ran, X.; Yan, X.; Yan, W.; Wang, Q.; Yin, T.; Zhou, J.G.; Hu, T.; Wang, G. Corrosion behavior and biocompatibility evaluation of a novel zinc-based alloy stent in rabbit carotid artery model. *J. Biomed. Mater. Res. Part B Appl. Biomater.* **2019**, *107*, 1814–1823. [CrossRef] [PubMed]
3. Gao, F.; Hu, Y.; Li, G.; Liu, S.; Quan, L.; Yang, Z.; Wei, Y.; Pan, C. Layer-by-layer deposition of bioactive layers on magnesium alloy stent materials to improve corrosion resistance and biocompatibility. *Bioact. Mater.* **2020**, *5*, 611–623. [CrossRef]
4. Ostrowski, N.J.; Lee, B.; Roy, A.; Ramanathan, M.; Kumta, P.N. Biodegradable poly(lactide-co-glycolide) coatings on magnesium alloys for orthopedic applications. *J. Mater. Sci.* **2013**, *24*, 85–96. [CrossRef] [PubMed]
5. Staiger, M.P.; Pietak, A.M.; Huadmai, J.; Dias, G. Magnesium and its alloys as orthopedic biomaterials: A review. *Biomaterials* **2006**, *27*, 1728–1734. [CrossRef] [PubMed]
6. Hanada, K.; Matsuzaki, K.; Huang, X.; Chino, Y. Fabrication of Mg alloy tubes for biodegradable stent application. *Mater. Sci. Eng. C* **2013**, *33*, 4746–4750. [CrossRef] [PubMed]
7. Salahshoor, M.; Guo, Y. Biodegradable orthopedic magnesium–calcium (MgCa) alloys, processing, and corrosion performance. *Materials* **2012**, *5*, 135–155. [CrossRef]
8. Witte, F.; Ulrich, H.; Rudert, M.; Willbold, E. Biodegradable magnesium scaffolds: Part 1: Appropriate inflammatory response. *J. Biomed. Mater. Res. Part A* **2007**, *81A*, 748–756. [CrossRef] [PubMed]
9. Aversa, R.; Petrescu, R.V.V.; Apicella, A.; Petrescu, F.I. Nano-Diamond Hybrid Materials for Structural Biomedical Application. *Am. J. Biochem. Biotechnol.* **2017**, *13*, 34–41. [CrossRef]
10. Windhagen, H.; Radtke, K.; Weizbauer, A.; Diekmann, J.; Noll, Y.; Kreimeyer, U.; Schavan, R.; Stukenborg-Colsman, C.; Waizy, H. Biodegradable magnesium-based screw clinically equivalent to titanium screw in hallux valgus surgery: Short term results of the first prospective, randomized, controlled clinical pilot study. *Biomed. Eng. Online* **2013**, *12*, 1–10. [CrossRef]
11. Wu, G.; Ibrahim, J.M.; Chu, P.K. Surface design of biodegradable magnesium alloys—A review. *Surf. Coat. Technol.* **2013**, *233*, 2–12. [CrossRef]
12. Chen, S.; Guan, S.; Li, W.; Wang, H.; Chen, J.; Wang, Y.; Wang, H. In vivo degradation and bone response of a composite coating on Mg-Zn-Ca alloy prepared by microarc oxidation and electrochemical deposition. *J. Biomed. Mater. Res. Part B Appl. Biomater.* **2012**, *100*, 533–543. [CrossRef] [PubMed]
13. Sezer, N.; Evis, Z.; Koç, M. Additive manufacturing of biodegradable magnesium implants and scaffolds: Review of the recent advances and research trends. *J. Magnes. Alloy* **2020**, *9*, 392–415. [CrossRef]

14. Aversa, R.; Petrescu, V.; Apicella, A.; Petrescu, I.T. The Basic Elements of Life's. *Am. J. Eng. Appl. Sci.* **2016**, *9*, 1189–1197. [CrossRef]
15. Aversa, R.; Tamburrino, F.; Petrescu, R.V.V.; Petrescu, F.I.; Artur, M.; Chen, G.; Apicella, A. Biomechanically Inspired Shape Memory Effect Machines Driven by Muscle like Acting NiTi Alloys. *Am. J. Appl. Sci.* **2016**, *13*, 1264–1271. [CrossRef]
16. Jacobs, J.J.; Hallab, N.J.; Skipor, A.K.; Urban, R.M. Metal Degradation Products: A Cause for Concern in Metal-Metal Bearings? *Clin. Orthop. Relat. Res.* **2003**, *417*, 139–147.
17. Granchi, D.; Ciapetti, G.; Stea, S.; Savarino, L.; Filippini, F.; Sudanese, A.; Zinghi, G.; Montanaro, L. Cytokine release in mononuclear cells of patients with Co–Cr hip prosthesis. *Biomaterials* **1999**, *20*, 1079–1086. [CrossRef]
18. Niki, Y.; Matsumoto, H.; Suda, Y.; Otani, T.; Fujikawa, K.; Toyama, Y.; Hisamori, N.; Nozue, A. Metal ions induce bone-resorbing cytokine production through the redox pathway in synoviocytes and bone marrow macrophages. *Biomaterials* **2003**, *24*, 1447–1457. [CrossRef]
19. Waizy, H.; Seitz, J.-M.; Reifenrath, J.; Weizbauer, A.; Bach, F.-W.; Meyer-Lindenberg, A.; Denkena, B.; Windhagen, H. Biodegradable magnesium implants for orthopedic applications. *J. Mater. Sci.* **2013**, *48*, 39–50. [CrossRef]
20. Xu, R.; Yang, X.; Suen, K.W.; Wu, G.; Li, P.; Chu, P.K. Improved corrosion resistance on biodegradable magnesium by zinc and aluminum ion implantation. *Appl. Surf. Sci.* **2012**, *263*, 608–612. [CrossRef]
21. Xin, Y.; Liu, C.; Zhang, X.; Tang, G.; Tian, X.; Chu, P.K. Corrosion behavior of biomedical AZ91 magnesium alloy in simulated body fluids. *J. Mater. Res.* **2007**, *22*, 2004–2011. [CrossRef]
22. Aversa, R.; Petrescu, R.V.V.; Petrescu, F.I.T.; Apicella, A. Biomimetic and evolutionary design driven innovation in sustainable products development. *Am. J. Eng. Appl. Sci.* **2016**, *9*, 1027–1036. [CrossRef]
23. Witte, F.; Fischer, J.; Nellesen, J.; Crostack, H.-A.; Kaese, V.; Pisch, A.; Beckmann, F.; Windhagen, H. In vitro and in vivo corrosion measurements of magnesium alloys. *Biomaterials* **2006**, *27*, 1013–1018. [CrossRef] [PubMed]
24. Li, L.; Gao, J.; Wang, Y. Evaluation of cyto-toxicity and corrosion behavior of alkali-heat-treated magnesium in simulated body fluid. *Surf. Coat. Technol.* **2004**, *185*, 92–98. [CrossRef]
25. Liu, C.; Xin, Y.; Tian, X.; Chu, P.K. Corrosion behavior of AZ91 magnesium alloy treated by plasma immersion ion implantation and deposition in artificial physiological fluids. *Thin Solid Film.* **2007**, *516*, 422–427. [CrossRef]
26. Wang, J.; Tang, J.; Zhang, P.; Li, Y.; Wang, J.; Lai, Y.; Qin, L. Surface modification of magnesium alloys developed for bioabsorbable orthopedic implants: A general review. *J. Biomed. Mater. Res. Part B Appl. Biomater.* **2012**, *100*, 1691–1701. [CrossRef]
27. Raffaella, A.; Petrescu, F.I.T.; Petrescu, R.V.V.; Antonio, A. Biomimetic finite element analysis bone modeling for customized hybrid biological prostheses development. *Am. J. Appl. Sci.* **2016**, *13*, 1060–1067. [CrossRef]
28. Wang, X.; Zeng, X.; Wu, G.; Yao, S.; Lai, Y. Effects of tantalum ion implantation on the corrosion behavior of AZ31 magnesium alloys. *J. Alloys Compd.* **2007**, *437*, 87–92. [CrossRef]
29. Zhou, H.; Chen, F.; Yang, Y.G.; Wan, H.C.; Cai, S. Study on Process of Ion Implantation on AZ31 Magnesium Alloy. *Key Eng. Mater.* **2008**, *373–374*, 342–345. [CrossRef]
30. Orlowski, M.; Ruebben, A. Bioresorbable Metal Stent with Controlled Resorption. U.S. Patent Application No. 12/524,702, 30 January 2008.
31. Bertsch, T.; Borck, A. Biocorrodible Metallic Implant Having a Coating or Cavity Filling Made of Gelatin. U.S. Patent Application No. 11/850,346, 6 March 2008.
32. Zharkova, I.I.; Staroverova, O.V.; Voinova, V.V.; Andreeva, N.V.; Shushckevich, A.M.; Sklyanchuk, E.D.; Kuzmicheva, G.M.; Bespalova, A.E.; Akulina, E.A.; Shaitan, K.V.; et al. Biocompatibility of electrospun poly(3-hydroxybutyrate) and its composites scaffolds for tissue engineering. *Biomeditsinskaya Khimiya* **2014**, *60*, 553–560. [CrossRef]
33. Adden, N. Implant of a Biocorrodable Magnesium Alloy and Having a Coating of a Biocorrodable Polyphosphazene. U.S. Patent Application No. 12/192,729, 19 February 2009.
34. Zhang, X.P.; Zhao, Z.P.; Wu, F.M.; Wang, Y.L.; Wu, J. Corrosion and wear resistance of AZ91D magnesium alloy with and without micro-arc oxidation coating in Hank's solution. *J. Mater. Sci.* **2007**, *42*, 8523–8528. [CrossRef]
35. Xu, X.; Lu, P.; Guo, M.; Fang, M. Cross-linked gelatin/nanoparticles composite coating on micro-arc oxidation film for corrosion and drug release. *Appl. Surf. Sci.* **2010**, *256*, 2367–2371. [CrossRef]
36. Jo, J.H.; Hong, J.Y.; Shin, K.S.; Kim, H.E.; Koh, Y.H. Enhancing biocompatibility and corrosion resistance of Mg implants via surface treatments. *J. Biomater. Appl.* **2012**, *27*, 469–476. [CrossRef]
37. Salunke, P.; Shanov, V.; Witte, F. High purity biodegradable magnesium coating for implant application. *Mater. Sci. Eng. B* **2011**, *176*, 1711–1717. [CrossRef]
38. Wong, H.M.; Yeung, K.W.K.; Lam, K.O.; Tam, V.; Chu, P.K.; Luk, K.D.K.; Cheung, K.M.C. A biodegradable polymer-based coating to control the performance of magnesium alloy orthopaedic implants. *Biomaterials* **2010**, *31*, 2084–2096. [CrossRef] [PubMed]
39. Aversa, R.; Petrescu, R.; Petrescu, F.; Perrotta, V.; Apicella, D.; Apicella, A. Biomechanically Tunable Nano-Silica/P-HEMA Structural Hydrogels for Bone Scaffolding. *Bioengineering* **2021**, *8*, 45. [CrossRef] [PubMed]
40. Witte, F.; Hort, N.; Vogt, C.; Cohen, S.; Kainer, K.U.; Willumeit, R.; Feyerabend, F. Degradable biomaterials based on magnesium corrosion. *Curr. Opin. Solid State Mater. Sci.* **2008**, *12*, 63–72. [CrossRef]
41. Gray-Munro, J.E.; Seguin, C.; Strong, M. Influence of surface modification on the in vitro corrosion rate of magnesium alloy AZ31. *J. Biomed. Mater. Res. Part A* **2009**, *91*, 221–230. [CrossRef]

42. Raffaella, A.; Petrescu, R.V.V.; Antonio, A.; Petrescu, F.I.T. Physiologic human fluids and swelling behavior of hydrophilic biocompatible hybrid ceramo-polymeric materials. *Am. J. Eng. Appl. Sci.* **2016**, *9*, 962–972. [CrossRef]
43. Gogolewski, S.; Jovanovic, M.; Perren, S.M.; Dillon, J.G.; Hughes, M.K. Tissue response and in vivo degradation of selected polyhydroxyacids: Polylactides (PLA), poly(3-hydroxybutyrate) (PHB), and poly(3-hydroxybutyrate-co-3-hydroxyvalerate) (PHB/VA). *J. Biomed. Mater. Res.* **1993**, *27*, 1135–1148. [CrossRef]
44. Kostopoulos, L.; Karring, T. Augmentation of the rat mandible using guided tissue regeneration. *Clin. Oral Implant. Res.* **1994**, *5*, 75–82. [CrossRef]
45. Shishatskaya, E.I.; Volova, T.G.; Gordeev, S.A.; Puzyr, A.P. Degradation of P(3HB) and P(3HB-co-3HV) in biological media. *J. Biomater. Sci. Polym. Ed.* **2005**, *16*, 643–657. [CrossRef] [PubMed]
46. Li, T.; Qi, K. Microbial Polyesters: The Polymer of the Future. *Explor. Nat.* **1994**, *13*, 35–41.
47. Baptist, J.N. Process for Preparing Poly β-Hyroxybutyric Acid. U.S. Patent Application No. 3044942, 17 July 1960.
48. Wang, Z.; Yan, J.; Zheng, Q.; Wang, Z. CyclinD1, CDK4, and P21 expression by IEC-6 cells in response to NiTi alloy and polymeric biomaterials. *Mater. Sci. Eng. C* **2012**, *32*, 2183–2189. [CrossRef]
49. Rahmany, M.B.; Van Dyke, M. Biomimetic approaches to modulate cellular adhesion in biomaterials: A review. *Acta Biomater.* **2013**, *9*, 5431–5437. [CrossRef]
50. Hornberger, H.; Virtanen, S.; Boccaccini, A. Biomedical coatings on magnesium alloys—A review. *Acta Biomater.* **2012**, *8*, 2442–2455. [CrossRef] [PubMed]
51. Mueller, P.P.; May, T.; Perz, A.; Hauser, H.; Peuster, M. Control of smooth muscle cell proliferation by ferrous iron. *Biomaterials* **2006**, *27*, 2193–2200. [CrossRef]
52. Walter, R.; Kannan, M.B. In-vitro degradation behaviour of WE54 magnesium alloy in simulated body fluid. *Mater. Lett.* **2011**, *65*, 748–750. [CrossRef]
53. Song, J.; Van Ooij, W.J. Bonding and corrosion protection mechanisms of gamma-APS and BTSE silane films on aluminum substrates. *J. Adhes. Sci. Technol.* **2003**, *17*, 2191–2221. [CrossRef]
54. Jones, D.A.; Amy, P.S. A Thermodynamic Interpretation of Microbiologically Influenced Corrosion. *Corrosion* **2002**, *58*, 638–645. [CrossRef]
55. Song, G.; Atrens, A. Understanding Magnesium Corrosion—A Framework for Improved Alloy Performance. *Adv. Eng. Mater.* **2003**, *5*, 837–858. [CrossRef]
56. Zhu, D.; van Ooij, W.J. Corrosion protection of AA 2024-T3 by bis-[3-(triethoxysilyl)propyl]tetrasulfide in sodium chloride solution.: Part 2: Mechanism for corrosion protection. *Corros. Sci.* **2003**, *45*, 2177–2197. [CrossRef]
57. Liu, X.; Yue, Z.; Romeo, T.; Weber, J.; Scheuermann, T.; Moulton, S.; Wallace, G. Biofunctionalized anti-corrosive silane coatings for magnesium alloys. *Acta Biomater.* **2013**, *9*, 8671–8677. [CrossRef] [PubMed]
58. Jyoti, G.; Keshav, A.; Anandkumar, J. Review on Pervaporation: Theory, Membrane Performance, and Application to Intensification of Esterification Reaction. *J. Eng.* **2015**, *2015*, 1–24. [CrossRef]
59. Ball, I.J.; Huang, S.; Wolf, R.A.; Shimano, J.Y.; Kaner, R.B. Pervaporation studies with polyaniline membranes and blends. *J. Membr. Sci.* **2000**, *174*, 161–176. [CrossRef]
60. Sawada, H.; Takahashi, Y.; Miyata, S.; Kanehashi, S.; Sato, S.; Nagai, K. Gas Transport Properties and Crystalline Structures of Poly(lactic acid) Membranes. *Trans. Mater. Res. Soc. Jpn.* **2010**, *35*, 241–246. [CrossRef]
61. Kawamura, N.; Nakao, Y.; Ishikawa, R.; Tsuchida, D.; Iijima, M. Degradation and Biocompatibility of AZ31 Magnesium Alloy Implants In Vitro and In Vivo: A Micro-Computed Tomography Study in Rats. *Materials* **2020**, *13*, 473. [CrossRef]
62. Leleu, S.; Rives, B.; Causse, N.; Pébère, N. Corrosion rate determination of rare-earth Mg alloys in a Na_2SO_4 solution by electrochemical measurements and inductive coupled plasma-optical emission spectroscopy. *J. Magnes. Alloy* **2019**, *7*, 47–57. [CrossRef]
63. Hofstetter, J.; Becker, M.; Martinelli, E.; Weinberg, A.M.; Mingler, B.; Kilian, H.; Pogatscher, S.; Uggowitzer, P.J.; Löffler, J.F. High-strength low-alloy (HSLA) Mg-Zn-Ca alloys with excellent biodegradation performance. *JOM* **2014**, *66*, 566–572. [CrossRef]
64. Holweg, P.; Berger, L.; Cihova, M.; Donohue, N.; Clement, B.; Schwarze, U.; Sommer, N.G.; Hohenberger, G.; van den Beucken, J.J.J.P.; Seibert, F.; et al. A lean magnesium–zinc–calcium alloy ZX00 used for bone fracture stabilization in a large growing-animal model. *Acta Biomater.* **2020**, *113*, 646–659. [CrossRef]
65. Rivard, C.H.; Chaput, C.; Rhalmi, S.; Selmani, A. Bio-absorbable synthetic polyesters and tissue regeneration. A study of three-dimensional proliferation of ovine chondrocytes and osteoblasts. *Ann. Chir.* **1996**, *50*, 651–658.
66. Sun, J.; Dai, Z.; Zhao, Y.; Chen, G.Q. In vitro effect of oligo-hydroxyalkanoates on the growth of mouse fibroblast cell line L929. *Biomaterials* **2007**, *28*, 3896–3903. [CrossRef] [PubMed]
67. Wang, Y.; Jiang, X.L.; Yang, S.C.; Lin, X.; He, Y.; Yan, C.; Wu, L.; Chen, G.Q.; Wang, Z.Y.; Wu, Q. MicroRNAs in the regulation of interfacial behaviors of MSCs cultured on microgrooved surface pattern. *Biomaterials* **2011**, *32*, 9207–9217. [CrossRef] [PubMed]
68. Chen, G.-Q.; Zhang, J. Microbial polyhydroxyalkanoates as medical implant biomaterials. *Artif. Cells Nanomed. Biotechnol.* **2018**, *46*, 1–18. [CrossRef] [PubMed]
69. Cheng, G.; Cai, Z.; Wang, L. Biocompatibility and biodegradation of poly(hydroxybutyrate)/poly(ethylene glycol) blend films. *J. Mater. Sci. Mater. Electron.* **2003**, *14*, 1073–1078. [CrossRef] [PubMed]
70. Liu, B.; Zheng, Y. Effects of alloying elements (Mn, Co, Al, W, Sn, B, C and S) on biodegradability and in vitro biocompatibility of pure iron. *Acta Biomater.* **2011**, *7*, 1407–1420. [CrossRef] [PubMed]

71. Ali, S.; Rani, A.M.A.; Baig, Z.; Ahmed, S.W.; Hussain, G.; Subramaniam, K.; Hastuty, S.; Rao, T.V. Biocompatibility and corrosion resistance of metallic biomaterials. *Corros. Rev.* **2020**, *38*, 381–402. [CrossRef]
72. Davide, A.; Raffaella, A.; Marco, T.; Michele, S.; Syed, J.; Massimo, M.; Marco, F.; Antonio, A.; Apicella, A. Direct restoration modalities of fractured central maxillary incisors: A multi-levels validated finite elements analysis with in vivo strain measurements. *Dent. Mater.* **2015**, *31*, e289–e305. [CrossRef]